

Article

Effect of Cold-Deformation on Austenite Grain Growth Behavior in Solution-Treated Low Alloy Steel

Xianguang Zhang ^{1,*}, Kiyotaka Matsuura ² and Munekazu Ohno ²

¹ School of Metallurgical and Ecological Engineering, University of Science and Technology Beijing (USTB), Beijing 100083, China

² Division of Materials Science and Engineering, Faculty of Engineering, Hokkaido University, Kita 13 Nishi 8, Kita-ku, Sapporo 060-8628, Hokkaido, Japan; matsuura@eng.hokudai.ac.jp (K.M.); mohno@eng.hokudai.ac.jp (M.O.)

* Correspondence: xgzhang@ustb.edu.cn; Tel.: +86-10-6233-2267

Received: 28 October 2018; Accepted: 21 November 2018; Published: 1 December 2018



Abstract: The occurrence of abnormal grain growth (AGG) of austenite during annealing is a serious problem in steels with carbide and/or nitride particles, which should be avoided from a viewpoint of mechanical properties. The effects of cold deformation prior to annealing on the occurrence of AGG have been investigated. It was found that the temperature range of the occurrence of AGG is shifted toward a low temperature region by cold deformation, and that the shift increases with the increase of the reduction ratio. The lowered AGG occurrence temperature is attributed to the fine and near-equilibrium AlN particles that are precipitated in the cold-deformed steel, which is readily dissolved during annealing. In contrast, coarse and non-equilibrium AlN particles precipitated in the undeformed steel, which is resistant to dissolution during annealing.

Keywords: austenite; abnormal grain growth; cold-deformation; precipitate

1. Introduction

Microalloying has been used as an important austenite grain refinement technology in steels. Austenite grain growth can be inhibited by microalloying, which causes the precipitation of second-phase particles in austenite [1–5]. Abnormal grain growth (AGG) frequently occurs in micro-alloyed steels during annealing. The austenite grain growth of the micro-alloyed steels usually experiences “normal → abnormal → normal” growth modes in sequence, with an increase of the annealing temperature [5]. AGG occurs within a certain temperature range during annealing, which is referred to as an AGG temperature range. The AGG temperature range of steels is an important factor in designing the heat treatment to achieve fine-grained products.

The austenite grain growth behavior in low-alloy steels is largely dependent on the stability of second-phase particles. At low temperatures, the second-phase particles are stable, and the austenite grain boundaries can be effectively pinned by the particles. The grain growth is thus greatly retarded. However, at relatively high temperatures, the second-phase particles become unstable, and they readily dissolve or coarsen [5]. Then, some of the austenite grains may become unpinned, and they may grow much faster than the matrix grains. This leads to the occurrence of AGG [6]. There is a transition temperature at which the austenite grain growth switches from normal grain growth (NGG) to AGG mode. This transition temperature is referred to as a grain coarsening temperature, T_c [7]. In addition, at temperatures that are much higher than the T_c , NGG resumes, due to the almost complete dissolution of the pinning particles, and the grain growth becomes free [5]. Hence, there is another transition temperature, the AGG finishing temperature (T_f), at which the grain growth

switches from AGG to NGG mode. T_c and T_f are important parameters for understanding the grain growth behavior of austenite.

Cold-deformation, such as cold-rolling, hammering, or cold-forging, has been widely used in the steel manufacturing process. It was found that hot-deformation could accelerate the nucleation and coarsening of the second-phase particles due to the large amount of dislocation that is introduced into the steels by deformation [8–10]. In addition, previous studies [11–13] have revealed that cold-deformation also has a strong influence on the precipitation and growth of the precipitates during subsequent annealing. It was found that the second-phase particles were finer and distributed more uniformly by cold-deformation [11]. Meanwhile, cold-deformation makes the precipitates resistant to coarsening [11,12].

The grain growth behavior of austenite relies on the presence of second-phase particles. Therefore, it is expected that the cold-deformation should have a strong influence on the AGG temperature range of the low-alloy steels. However, previous works have mainly focused on the effect of cold-deformation on the precipitation or coarsening behaviors of second-phase particles. Rare attention has been paid to its influence on austenite grain growth behavior. Recently, it was reported by the present authors [13,14] that an inhomogeneous distribution of AlN particles in ferrite/pearlite banded steel became homogeneous, due to cold-deformation prior to austenization, which increased the low T_c of the banded steel significantly. However, to the best of the authors' knowledge, no systematic work has been reported regarding the effects of cold deformation on the AGG temperature range of austenite. The present study has been undertaken to clarify the effects of cold-deformation on austenite grain growth behavior in solution-treated low-alloy steel. It was found that the AGG temperature range of austenite is shifted toward the lower temperature region by applying prior cold-deformation.

2. Materials and Methods

The composition of the low-alloy steel used in the present study is displayed in Table 1. The solubility of AlN in austenite can be written as [15]:

$$\text{Log}[\text{Al}][\text{N}] = 1.03 - 6770/T \quad (1)$$

Where [Al] and [N] represent the solubilities of aluminum and nitrogen at the absolute temperature T . According to Equation (1), the complete dissolution temperature of AlN in the current steel was calculated to be 1453 K. To completely dissolve the AlN, and to eliminate the banded segregation of Mn, the solution treatment temperature and time was designed to be 1573 K for 2 h. After the solution treatment, the specimen was air-cooled to room temperature.

Table 1. Composition of the steel used in this study (wt %).

C	Mn	Si	P	Al	N	Fe
0.2	0.8	0.2	0.015	0.04	0.006	Bal.

The cold-deformation was carried out by cold-rolling, with reduction ratios ranging from 10 to 70%. Both the solution-treated (ST), and solution-treated and deformed (STD) specimens were annealed at temperatures between 1173–1473 K for various periods, as schematically shown in Figure 1. The heating rate of the specimens was about 5 K/s. After annealing, the specimens were quenched in ice water to freeze the microstructure. The specimens were cut and mechanically polished to obtain a mirror-like surface. To reveal the prior austenite grain boundaries, the specimens were etched in a supersaturated picric acid solution at 333 K. The microstructure was characterized by using an optical microscope (OM). The well-known linear intercept method was used to evaluate the mean austenite grain size. About 450 to 550 intercepts were counted for each sample.

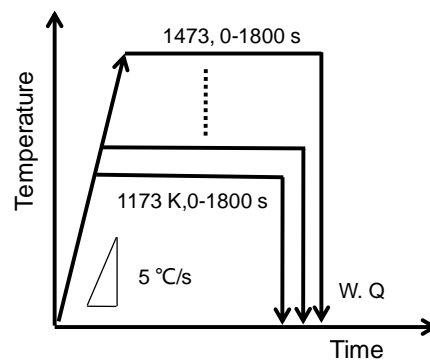


Figure 1. Schematic illustrations of the annealing treatment.

The AlN particles were characterized by using transmission electron microscopy (TEM, JEOL JEM-2010, JEOL Ltd., Tokyo, Japan) equipped with energy dispersive spectroscopy (EDS) operating at 200 kV on carbon extraction replicas eroded off the specimens. At least a thousand AlN precipitates were measured for each case to evaluate the volume fraction and particle sizes.

The volume fraction of the AlN precipitates from the carbon extraction replica can be calculated based on the McCall-Boyed method [16] as follows:

$$f = \left(\frac{1.4\pi}{6} \right) \left(\frac{ND^3}{V} \right), \quad (2)$$

where N is the number of the precipitates, D is the mean diameter of the particles, and V is the volume of the matrix from which the precipitates were extracted. The thickness of the matrix can be assumed as the mean diameter of the particles [17]. Thus, Equation (2) can be written as:

$$f = \left(\frac{1.4\pi}{6} \right) \left(\frac{ND^2}{S} \right), \quad (3)$$

where S is the area of the corresponding matrix.

3. Results and Discussion

3.1. Austenite Grain Growth Behavior

Figure 2 shows the prior austenite grain structures (now martensite after quenching) of the solution-treated (ST) specimens after annealing at different temperatures for various periods of time. Microstructure observation revealed that the austenite grain growth during annealing at 1298 K is very slow and the prior austenite grain size almost has no change. Hence, only the microstructure after annealing at 1298 K for 1800 s is shown Figure 2a. It is clear that fine and uniform prior austenite grain structures were formed, which is attributed to the occurrence of NGG. However, mixed prior austenite grain structures were formed after the specimen was annealed at 1323 K for 60 s, as shown in Figure 2b, where abnormal coarse grain (as indicated by the red arrow) mixed with fine matrix grain structures (as indicated by the black arrow) were observed. After a prolonged holding time of up to 1800 s, extremely coarse grain structures were developed (Figure 2c). Hence, typical AGG occurred at this temperature. After the sample was annealed at 1423 K for 1800 s, slightly coarse but uniform grain structures were formed (Figure 2d). This indicates that the grain growth switched to NGG mode again.

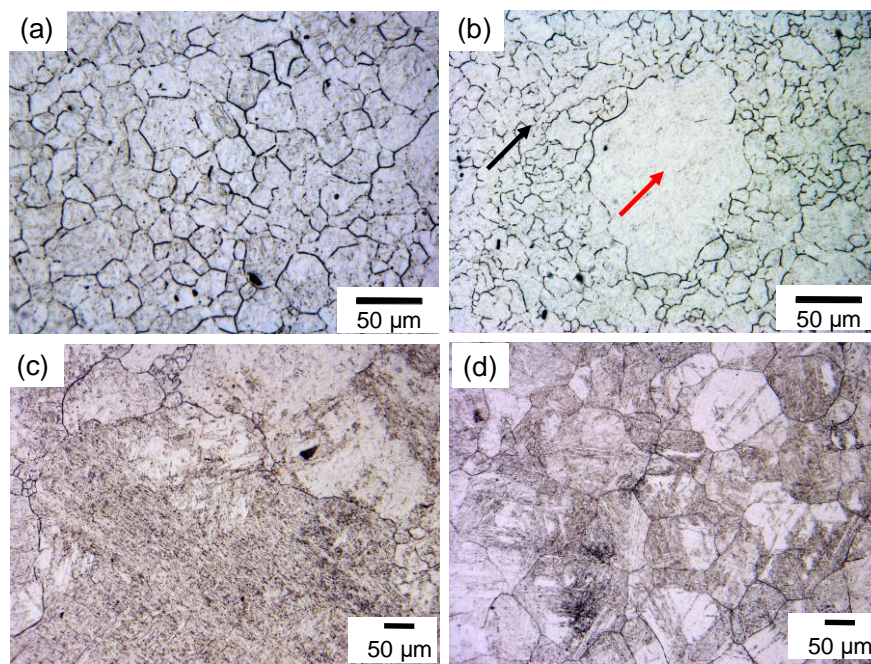


Figure 2. Prior austenite grain structures of the solution-treated (ST) specimens after annealing at (a) 1298 K for 1800 s, (b) 1323 K for 60 s, (c) 1323 K for 1800 s, and (d) 1423 K for 1800 s. The red and black arrows in (b) to indicate the abnormal coarse and fine matrix grains, respectively.

According to the above results, the occurrence AGG led to extremely coarse grain structures, while the NGG led to relatively fine grain structures after annealing. Therefore, the mean austenite grain size of the ST specimens after annealed at various temperatures for 1800 s were plotted in Figure 3a to show the austenite grain growth behavior during annealing. The average austenite grain sizes after annealing at 1298 K (Figure 2a), 1323 K (Figure 2c), and 1423 K (Figure 2d) are indicated by a black solid, red solid, and open arrows, correspondingly. From Figure 3a, it can be seen that the prior austenite grain size is fine, and that it has almost no change below 1298 K. This indicates that the austenite grain growth was greatly retarded, and it grew under the NGG mode below 1298 K. The coarse grains that were formed by AGG appeared at intermediate temperatures. Slightly coarse grains that were formed by NGG appeared at high temperatures. Therefore, the ST specimens experienced “normal → abnormal → normal” grain growth modes that were usually observed in the micro-alloyed steels [5]. The grain growth modes and the transition temperatures of T_c and T_f are indicated in Figure 3a. It is necessary to point out that the grain growth behaviors were examined carefully by changing the annealing temperatures within 25 K intervals, and that only partial results are shown in Figure 3a.

To understand the effects of cold-deformation on the austenite grain growth behavior, the average austenite grain sizes at various temperatures in the solution-treated and cold-deformed by 50% (STD-50%) specimens were examined. The measured austenite grain size as a function of annealing temperature is summarized in Figure 3b. A similar grain structure changing tendency was observed as in that of the ST specimens; viz., a fine grain structure at low temperatures, a coarse grain structure at intermediate temperatures, and slightly coarse and uniform grain structures at high temperatures. Therefore, the STD-50% specimen experienced “normal → abnormal → normal” grain growth modes as well. The prior austenite grain structure evolution process was similar to that of the ST specimens, but at different temperatures; therefore, the microstructures are not shown here again. Importantly, comparing Figure 3a,b shows that the AGG temperature range was shifted toward a low temperature by cold-deformation.

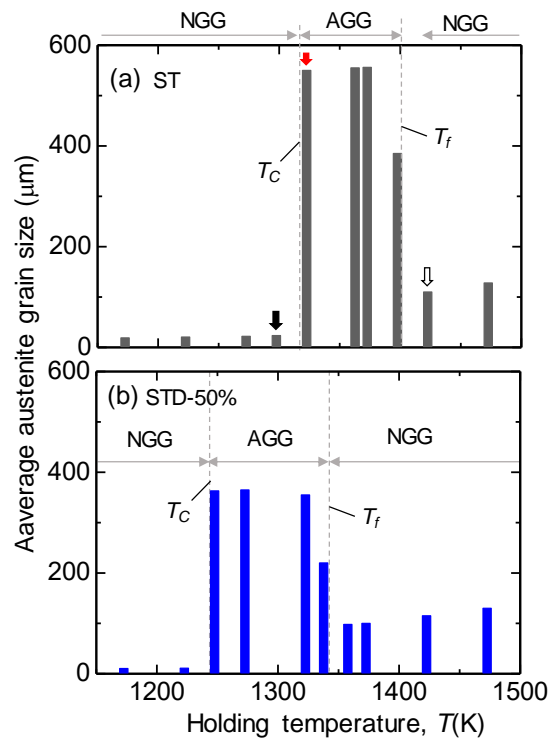


Figure 3. Average prior austenite grain sizes of the (a) ST and (b) solution-treated and cold-deformed by 50% (STD-50%) specimens after annealing at various temperatures for 1800 s.

To gain an overall image of the effect of cold-deformation on austenite grain growth behavior, the austenite grain growth modes against annealing temperatures in the specimens deformed with various reduction ratios are summarized in Figure 4. The “normal → abnormal → normal” grain growth modes occurred in all the specimens. Importantly, the AGG temperature range was gradually depressed toward low temperatures with the increase in the reduction ratio, which was almost saturated up to 70%. The decreased T_c and T_f temperatures, induced by the cold-deformation, can be explained by its influences on the evolution of the AlN precipitates, which is discussed in the following section.

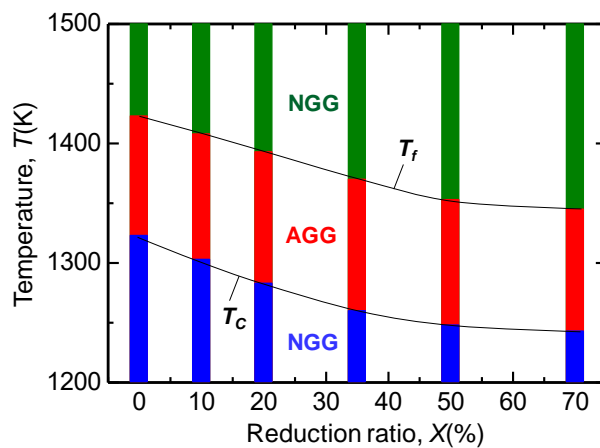


Figure 4. Austenite grain growth behavior against annealing temperatures in the specimens deformed at various reduction ratios.

3.2. The Evolution of AlN Precipitates

As reviewed in the Introduction, the stability of the second-phase particles during annealing plays a key role in the austenite grain growth behavior. To understand the reasons for the suppression of the

AGG temperature range by the cold-deformation, the evolution of the AlN particles were carefully studied by TEM observations. The volume fractions and sizes of the AlN particles in both the ST and STD-50% specimens quenched from various temperatures from 1073 to 1353 K are summarized in Figure 5a,b, respectively. For comparison, the equilibrium volume fraction of the AlN particles calculated from Equation (1) is also plotted in Figure 5a, as shown by the blue broken line.

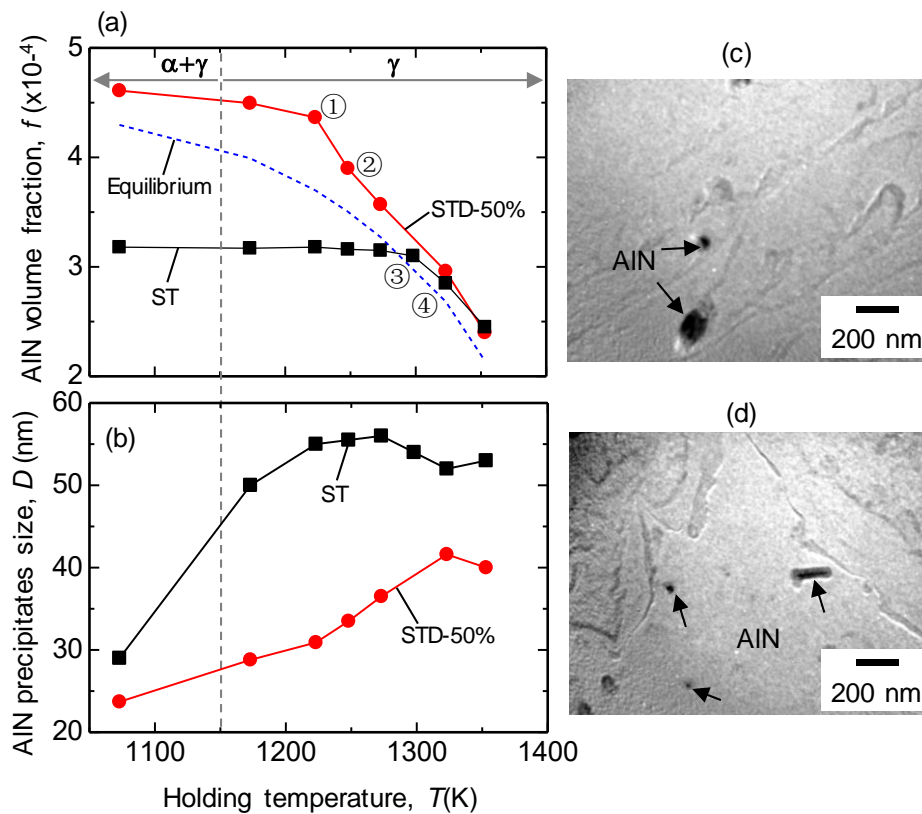


Figure 5. (a) Volume fraction and (b) size of the AlN particles in the ST and STD-50% specimens after annealing at various temperatures for 1800 s. TEM images of the AlN particles (indicated by the black arrows) in (c) ST and (d) STD-50% specimens after annealing at 1173 K for 1800 s.

It should be pointed out that after the solution treatment, the AlN precipitates should have been fully dissolved into the austenite. It was reported that the precipitation of AlN is difficult during the cooling process, and that it is sensitive to the cooling rate [18–20]. The precipitation of AlN can be entirely suppressed at a cooling rate larger than 1 K/s [21], which is approximately equivalent to air cooling a 50 mm diameter steel bar [22]. Therefore, the AlN precipitation during the air-cooling process is negligible in this study. The AlN precipitates should mainly be re-precipitated during the reheating process in both the ST and STD specimens.

According to the precipitation-time-temperature (PTT) diagram of AlN [23], the AlN precipitation should have been completed below 1073 K in the current steel during the annealing process. Therefore, the AlN particles within the specimens quenched from 1073 K (ferrite + austenite two phase region) were examined. According to Figure 5a,b, fine- and near-equilibrium AlN particles precipitated in the STD-50% specimen at 1073 K. Meanwhile, a much lower volume fraction of the AlN particles than the equilibrium was precipitated in the ST specimen. These indicate that the AlN particles have been almost fully precipitated in the STD-50% specimen, while the AlN particles were only partially been precipitated in the ST specimen. The near-equilibrium precipitation in the STD-50% specimen should result from the dislocation-induced precipitation of AlN [11]. It needs to point out that the slightly overestimated AlN volume fraction in the STD-50% specimen compared to the

equilibrium prediction should be caused by the differences between the metallographic observation and theoretical calculation.

It is necessary to point out that as the annealing temperature was raised up to 1173 K (just after the ferrite-to-austenite transformation), the AlN particles in the STD-50% specimen were less coarsened than that of the ST specimen (Figure 5b). This could be more clearly seen from the TEM images of the AlN particles in both the undeformed and cold-deformed specimens after annealing at 1173 K for 1800 s, as shown in Figure 5c,d, respectively. Smaller AlN particles were formed in the STD-50% specimen, than that of the ST specimen. Therefore, the AlN particles in the prior cold-deformed specimen had sluggish growth kinetics. This may strongly influence the dissolution behavior of the precipitates at high temperatures. Similar phenomena have also been reported by Furubayashi et al. [11] and Kesternich [12], while the mechanism(s) for this are still not very clear.

Regarding the pinning effect of the second-phase particles, there is a maximum radius of the precipitates, r_{crit} , for pinning the grain growth [6]. That is, only the fine second phase particles with a radius smaller than r_{crit} , can effectively pin the grain boundaries. The r_{crit} can be expressed as [6]:

$$r_{\text{crit}} = 3 \frac{R_0 f}{\pi} (3 - 4/Z)^{-1}, \quad (4)$$

where R_0 is the average grain size, Z is a parameter that is used to represent the inhomogeneity of the initial grains, and f is the volume fraction of second-phase particles. It is obvious that for a given uniform initial grain structure, r_{crit} linearly decreases with the decrease of f [6].

According to Figure 5a, the fraction of the AlN particles is stable in the STD-50% specimen below 1223 K (as indicated by symbol ① in Figure 5a). Therefore, both the r_{crit} and the pinning force, which is proportional to f/r [6] (here, r is the average radius of the pinning particles), may have no obvious change, and the grain boundaries can be well-pinned. This results in the sluggish austenite grain growth kinetics in the STD-50% specimens below 1223 K, as shown in Figure 3b. However, when the annealing temperature was increased up to 1248 K (position ② in Figure 5a), the fraction of the AlN particles in the STD-50% specimen decreased obviously. This may be caused by the accelerated diffusion rates of the elements at elevated temperatures, the increased solubility of the AlN in austenite, and the easy dissolution of the fine AlN particles in the STD-50% specimen. Hence, the r_{crit} may decrease, according to Equation (4). Then, the volume fraction of the AlN precipitates available to pin the grain boundaries may decrease steeply at 1248 K. This may cause the occurrence of AGG at this temperature.

As for the ST specimen, the fraction of AlN particles were almost constant until 1298 K (position ③ in Figure 5a). Therefore, both r_{crit} and the pinning force were stable, and thus the grain growth could be effectively retarded. This agrees with the observed sluggish grain growth kinetics below 1298 K in Figure 3a. However, as the annealing temperature was raised up to 1323 K (position ④ in Figure 5a), the fractions of the AlN particles were decreased, and the r_{crit} may decrease accordingly. This may result in the occurrence of AGG in the ST specimen, as shown in Figure 2b,c.

According to the discussion above, it can be concluded that the change in the volume fraction of the AlN particles during annealing plays a key role in the austenite grain growth behavior. The rapid decrease in the AlN volume fraction may greatly change the r_{crit} , and then the effective volume fraction of the second phase particles to pin the grain boundaries may decrease dramatically, which may result in the occurrence of AGG.

As reviewed in the Introduction, the transition from AGG to NGG mode occurs at high temperatures when the AlN precipitates are nearly completely dissolved, and the grain growth becomes free. According to Figure 5a, the fractions of the AlN particles in both the deformed and undeformed specimens were low at 1353 K. Experimental results revealed that AGG occurred within 60 s when the ST specimen was annealed at 1353 K, while NGG occurred in the STD-50% specimen, even after a longer holding time (Figure 3b). The average diameters of the AlN particles in ST and STD-50% specimens after annealing at 1353 K for 0 s were evaluated to be around 60 and 30 nm,

correspondingly. It was reported that the dissolution time and the size of the precipitates had a parabolic relationship [23]. Accordingly, the dissolution time of the AlN particles in the ST specimen was around four times that in the STD-50% specimen. Therefore, it was possible that the fine AlN precipitates in the STD-50% specimen dissolved very quickly during annealing, which made the grain growth become free and change to the NGG mode. However, since the dissolution of the coarse precipitates in the ST specimen took a longer time, AGG could occur. To quickly dissolve the relatively large AlN precipitates in the ST specimen, this required higher temperatures. This may promote the AGG-to-NGG transition temperature to the higher temperature in the ST specimen.

According to the above discussion, cold-deformation results in the fine and near-equilibrium precipitation of the AlN particles, which are readily dissolved during the heating process, due to the increase in the solubilities of Al and N in austenite. However, non-equilibrium and coarse AlN precipitates formed in the undeformed specimen, which were resistant to dissolution during the heating process. These should be the reasons for the suppression of the AGG temperature range by the prior cold-deformation.

4. Summary

In summary, the study of austenite grain growth behavior in a solution-treated low-alloy steel has shown that cold-deformation prior to annealing shifts the abnormal grain growth (AGG) temperature range of austenite toward a lower temperature region. The amount of shift increases with the increase of the reduction ratio. The lowered AGG occurrence temperature is attributed to the effects of cold deformation on the evolution of the AlN precipitates during annealing. TEM observations confirmed that a much lower volume fraction than the equilibrium and coarse AlN precipitates formed in the undeformed steel, which is resistant to dissolution during annealing. However, prior cold-deformation results in the fine and near-equilibrium precipitation of AlN, which is readily dissolved at elevated temperatures. This results in the shift of the AGG temperature range to lower temperatures from the application of prior cold-deformation.

Author Contributions: X.Z., K.M. and M.O. conceived and designed the experiments; X.Z. performed the experiments and collected the data; X.Z., and K.M. analyzed the data; X.Z. wrote the paper; K.M. and M.O. discussed with the results and revised the manuscript.

Funding: This work was partially supported by “Nanotechnology Platform” Program of the Ministry of Education, Culture, Sports, Science and Technology (MEXT), Japan.

Conflicts of Interest: The authors declare no conflict of interest.

References

1. Morrison, W.B. Influence of small niobium additions on properties of carbon-manganese steels. *J. Iron Steel Inst.* **1963**, *201*, 317–325.
2. Webster, D.; Woodhead, J.H. Effect of 0.03 percent niobium on ferrite grain size of mild steel. *J. Iron Steel Inst.* **1964**, *202*, 987–994.
3. Irvine, K.J.; Pickering, F.B. Impact properties of low carbon bainitic steels. *J. Iron Steel Inst.* **1963**, *201*, 944–960.
4. Irvine, K.J.; Pickering, F.B.; Gladman, T. Grain-refined C-Mn steels. *J. Iron Steel Inst.* **1967**, *205*, 161–182.
5. Doğan, Ö.N.; Michal, G.M.; Kwon, H.W. Pinning of austenite grain boundaries by AlN precipitates and abnormal grain growth. *Metall. Trans. A* **1992**, *23*, 2121–2129. [[CrossRef](#)]
6. Gladman, T. On the theory of the effect of precipitate particles on grain growth in metals. *Proc. R. Soc.* **1966**, *294*, 298–309. [[CrossRef](#)]
7. Cuddy, L.J.; Raley, J.C. Austenite grain coarsening in microalloyed steels. *Metall. Trans. A* **1983**, *14*, 1989–1995. [[CrossRef](#)]
8. Dutta, B.; Palmiere, E.J.; Sellars, C.M. Modelling the kinetics of strain induced precipitation in Nb microalloyed steels. *Acta Mater.* **2001**, *49*, 785–794. [[CrossRef](#)]
9. Palmiere, E.J.; Garcia, C.I.; DeArdo, A.J. Compositional and microstructural changes which attend reheating and grain coarsening in steels containing niobium. *Metall. Mater. Trans. A* **1994**, *25*, 277–286. [[CrossRef](#)]

10. Liu, W.J. A new theory and kinetic modeling of strain-induced precipitation of Nb (CN) in microalloyed austenite. *Metall. Mater. Trans. A* **1995**, *26*, 1641–1657. [[CrossRef](#)]
11. Furubayashi, E.; Endo, H.; Yoshida, H. Effects of prior plastic deformation on the distribution and morphology of AlN precipitates in α iron. *Mater. Sci. Eng.* **1974**, *14*, 123–130. [[CrossRef](#)]
12. Kesternich, W. Dislocation-controlled precipitation of TiC particles and their resistance to coarsening. *Philos. Mag. A* **1985**, *52*, 533–548. [[CrossRef](#)]
13. Zhang, X.; Matsuura, K.; Ohno, M. Increase of austenite grain coarsening temperature in banded ferrite/pearlite steel by cold deformation. *Metall. Mater. Trans. A* **2015**, *46*, 32–36. [[CrossRef](#)]
14. Zhang, X.; Matsuura, K.; Ohno, M. Abnormal grain growth in austenite structure reversely transformed from ferrite/pearlite-banded structure. *Metall. Mater. Trans. A* **2014**, *45*, 4623–4634. [[CrossRef](#)]
15. Leslie, W.C.; Rickett, R.L.; Dotson, C.L.; Walton, C.S. Solution and precipitation of aluminum nitride in relation to the structure of low carbon steels. *Trans. Am. Soc. Met.* **1954**, *46*, 1470–1499.
16. McCall, J.L.; Boyd, J.E. Quantitative metallography of dispersion-strengthened alloys from extraction replicas-volume fraction and interparticle spacing. In Proceedings of the First Annual Technical Meeting of the International Metallographic Society, Denver, CO, USA, 8 September 1969; p. 153.
17. Ma, H.; Li, Y. Measure of size distribution and volume fraction of precipitates in silicon steel. *Mater. Sci. Eng.* **2002**, *20*, 328–330. (In Chinese)
18. Wilson, F.G.; Gladman, T. Aluminium nitride in steel. *Int. Mater. Rev.* **1988**, *33*, 221–286. [[CrossRef](#)]
19. Gladman, T.; Pickering, F.B. Grain-coarsening of austenite. *J. Iron Steel Inst.* **1967**, *205*, 653–664.
20. Hannerz, N.E. Influence of cooling rate and composition on intergranular fracture of cast steel. *Met. Sci. J.* **1968**, *2*, 148–152. [[CrossRef](#)]
21. Honer, K.E.; Baliktay, S. Susceptibility of steel castings to aluminium nitride-induced primary grain boundary fracture. In Proceedings of the 44th International Foundry Congress, Florence, Italy, 11–14 September 1977; pp. 125–140.
22. Atkins, M. *Atlas of Continuous Cooling Transformation Diagrams for Engineering Steels*; ASM International: Novelt, OH, USA, 1980.
23. Chen, Y.L.; Wang, Y.; Zhao, A.M. Precipitation of AlN and MnS in low carbon aluminium-killed steel. *J. Iron Steel Res. Int.* **2012**, *19*, 51–56. [[CrossRef](#)]



© 2018 by the authors. Licensee MDPI, Basel, Switzerland. This article is an open access article distributed under the terms and conditions of the Creative Commons Attribution (CC BY) license (<http://creativecommons.org/licenses/by/4.0/>).